Materials Letters 279 (2020) 128508

Contents lists available at ScienceDirect

Materials Letters

journal homepage: www.elsevier.com/locate/mlblue

First- and second-order phase transitions in Fe-(17-19)at.%Ga alloys

A.K. Mohamed [a,*], V.V. Cheverikin [a], S.V. Medvedeva [a], I.A. Bobrikov [b], A.M. Balagurov [b,c], I.S. Golovin [a,*]

[a] National University of Science and Technology "MISIS", Leninsky ave. 4, 119049 Moscow, Russia
[b] Frank Laboratory of Neutron Physics, Joint Institute for Nuclear Research, 141980 Dubna, Russia
[c] Lomonosov Moscow State University, 119991 Moscow, Russia

ARTICLE INFO

Article history:
Received 2 August 2020
Received in revised form 8 August 2020
Accepted 10 August 2020
Available online 12 August 2020

Keywords:
Fe-Ga
Phase transformations
Cooling rates
Grain boundaries
TTT diagram
Diffusion

ABSTRACT

The structure of the Fe-(17.5–19.5)at.%Ga alloys in as-cast and nearly equilibrium states is studied using XRD, ND, and EBSD. In disagreement with the existing phase diagrams, the long-term isothermally annealed at 450–500 °C Fe-17.5%Ga alloy has a two-phase structure with two co-existing ferromagnetic phases: bcc-originated A2($D0_3$) as a matrix and a fcc-originated A1($L1_2$) needle-shaped precipitates. The phase transitions during cooling of 17.5 and 19.5%Ga alloys from the A2 range of the phase diagram with different cooling rates were used to plot, at least partly, Time-Temperature-Transformation (TTT) diagrams. The critical cooling rates for starting first- and second-order transitions are determined for the Fe-19.5%Ga alloy. The effect of long-term annealing on magnetostriction is reported.

1. Introduction

The discovery of adding gallium to iron, which leads to enhancing the magnetostriction of iron by order of magnitude [1–3], has created a novel design model for devices that utilize magnetostrictive materials. There are two maxima for magnetostriction, depending on the Ga content in α-Fe [4]. The functional properties are extremely sensitive to the phases present in the alloy [5,6]. The cooling rate has an obvious effect on phase transitions from a high-temperature A2 phase to less metastable or equilibrium phases in the Fe-27 Ga alloy [7,8]. It is believed that alloys with 17-19at.%Ga do not exhibit first-order phase transitions that decrease magnetostriction. Here, we demonstrate that this is not true, and even in the alloy with as low Ga% as 17.5at.%, the first-order transition occurs both at instant slow cooling or long-term isothermal annealing. Consequently, the existing phase diagrams [9] need to be corrected.

2. Material and methods

Three alloys with nominal compositions Fe-17, 18, and 19%Ga (in this paper, we use only atomic %) were studied in this work. The alloys were produced by induction melting for Fe (commercial purity) and Ga (99.99%) under protective high-purity argon gas followed by casting and rapid solidification in a copper mold (4 × 16 × 60 mm) using an Indutherm MC-20 V mini furnace. The chemical composition analysis by Energy Dispersive X-ray Spectroscopy (EDX) revealed the following compositions: Fe-17.5 ± 0.1%, Fe-18.6 ± 0.1%, and Fe-19.5 ± 0.1%Ga.

The neutron diffraction (ND) patterns were measured at a high-resolution Fourier diffractometer [9], which operates at the IBR-2 pulsed reactor at JINR (Dubna). The time-of-flight of the instrument can be easily switched between high-resolution ($\Delta d/d \approx 0.0015$) and high-intensity ($\Delta d/d \approx 0.015$) diffraction modes.

The samples dimensions used for XRD and SEM-EBSD analyses are 10 × 10 × 2 mm, and for ND, they are 30 × 8 × 4 mm. The cooling rates of 1, 2, 4, and 8 °C/min were chosen for the *in situ* ND tests performed in a vacuum furnace. The cooling path for these tests in *in situ* ND from 850 to ≈250 °C is linear. Below 200 °C, the furnace follows slower natural cooling. The phase transitions below 200 °C can be neglected as they are very slow in Fe-Ga alloys [10,11].

For long-term annealing, the samples were evacuated in quartz ampules. The heat treatments were conducted in argon atmosphere (99.999%-purity) for 300 h at chosen temperatures between 300 and 575 °C ± 1 °C, followed by air-cooling.

3. Results and discussion

All the samples have a single A2 phase in the as-cast state in agreement with the relevant literature, including our recent study [7,12]. In this paper, we used three types of experiments to study

* Corresponding authors at: Leninsky ave. 4, 119049 Moscow, Russia.
E-mail addresses: abdelkarim.abdelkarim@feng.bu.edu.eg (A.K. Mohamed), i.golovin@misis.ru (I.S. Golovin).

https://doi.org/10.1016/j.matlet.2020.128508
0167-577X/

transitions in the supercooled A2 (α-Fe-Ga solid solution) phase, namely:

1. XRD study of the samples' structure after cooling down from 850 °C with different rates (from 0.8 to 2000 °C/min);
2. *In situ* ND study of the phase transitions during cooling from 850 °C with cooling rates between 1 and 8 °C/min;
3. Study the samples' structure after long-term isothermal annealing in a temperature range of 300–575 °C using XRD and SEM-EBSD analyses.

The first TTT diagram for the Fe-Ga alloy with 27%Ga was reported in [8]. There are two differences between the present study of the Fe-(17-19)Ga alloys and the alloy with 27%Ga:

i) according to the equilibrium phase diagram, the appearance of the $L1_2$ phase is not expected in alloys with Ga less than 18%, especially below 450 °C [9,13–15],
ii) first-order transition in Fe-(18–19)Ga is slower than that of in Fe-27 Ga.

Typical second-order transition in 17–19%Ga is the A2 → $D0_3$ as reported in many papers but the A2 → B2 transition is also mentioned in several studies, e.g. [16]. As an example, the dependencies of intensities of some fundamental (A2) and superstructure ($D0_3$) peaks as functions of temperature for the cooling rate of 2 °C/min for Fe-19.5%Ga are shown in Fig. 1a. The dependencies are similar for the cooling rates of 1, 4, and 8 °C/min. The appearance of superstructure peaks clearly indicates the formation of the ordered $D0_3$ structure at cooling. The ordering temperature for a chosen cooling rate can be more accurately determined from the behavior of the lattice constant (Fig. 1b). The dependence $a(T)$ clearly illustrates a decrease of the lattice constant under transition between disordered and ordered states (see, e.g. [17]). Though the transition is stretched over the temperature range, its beginning can be accurately determined. For 1, 2, 4, and 8 °C/min cooling rates ordering starts between 490 and 470 °C and ends between 420 and 400 °C (with accuracy ± 10 °C). Weak peaks of the fcc A1 phase (less than 1%) appear in the ND patterns after cooling with 1 and 2 °C/min. Ordering of the A1 phase in Fe-Ga leads to the formation of the $L1_2$ phase [18]. In the case of a small amount of the fcc phase, the superstructural peaks are too small, and it is impossible to distinguish between the A1 and $L1_2$ phases.

To trace the A2 → A1($L1_2$) transition, an XRD study of long-term annealed samples was used. The results are shown by pie charts (Fig. 2a) on the Fe-Ga equilibrium phase diagram [9]. The red color represents the $L1_2$ phase fraction. Fig. 2b shows the XRD patterns for Fe-17.5 Ga, 300 h annealed samples at 450, 500 °C and Fe-19.5 Ga at 575 °C. The contribution of the A1($L1_2$) phase (1 1 1) peak is obvious. The intensities are re-scaled in the logarithmic scale in the insets.

The microstructural investigation of the 300 h annealed Fe-17.5 Ga sample at 450 °C shows a bcc A2($D0_3$) phase matrix with needle-shaped precipitates (Fig. 2c,d). These precipitates correspond to the equilibrium A1($L1_2$) phase located at the grain boundaries and inside grains. Fig. 2(e,f) show the SEM-EBSD image for the 300 h annealed Fe-18.6 Ga sample at 575 °C with a similar microstructure with the $L1_2$ phase located mainly at the grain boundaries possibly due to mechanism discussed in [19]. The $L1_2$ needle-shaped precipitates inside grains and at the grain boundaries are presented in the SEM images for 300 h annealed samples of Fe-18.6 Ga at 500 °C, Fe-19.5 Ga at 450, 500, and 575 °C with two different magnifications Fig. 2(g-j).

The magnetostriction ($3/2\lambda$) for water quenched and long-term annealed at 400 °C Fe-17.5 Ga samples is shown in Fig. 2k. After high-temperature annealing followed by quenching (2000 °C/min), the Fe-19.5 Ga alloy shows a maximum $3/2\lambda_s$ value 94.6 ppm, and it is 74.5 ppm in Fe-17.5 Ga, both with the A2 structure. Long-term annealing of the Fe-17.5 Ga alloy decreases magnetostriction of the as quenched sample to 48.3 ppm.

The above discussed results are used to build the TTT diagrams for the Fe-17.5 Ga and Fe-19.5 Ga alloys (Fig. 3(a,b)). These diagrams include experimental points obtained by three types of tests: 1, 2, and 3. We reported in [20] that the air-cooled and quenched Fe-19 Ga samples do not exhibit any degree of ordering, and we use these results to identify the critical cooling rate for ordering. The experiments (1) with different cooling rates conclude that the critical cooling rate for the ordering start is 65 °C/min (green dashed line) and for the metastable A2 phase to equilibrium A2 + $D0_3$ + A1($L1_2$), the phase transition is 2 °C/min (red solid line). The blue points in Fig. 3b represent the ordering start and finish at cooling rates: 1–8 °C/min. For the Fe-17.5 Ga alloy, the C-shaped curve is introduced as a sketch: even 300 h annealing is insufficient to achieve the equilibrium state (Fig. 3a). Our further research aims to significantly increase the annealing time to precise the positions of the C-curves.

Thus these TTT diagrams for Fe-(17, 19)%Ga alloys (Fig. 3) develop the idea of creating maps of phase transitions in Fe-Ga alloys proposed in [7] and they are useful for practical applications.

4. Conclusions

The structure of the Fe-(17.5–19.5)%Ga alloys was studied during cooling with different rates and after long-term annealing by XRD, *in situ* ND, and SEM-EBSD. The effect of the cooling rate on

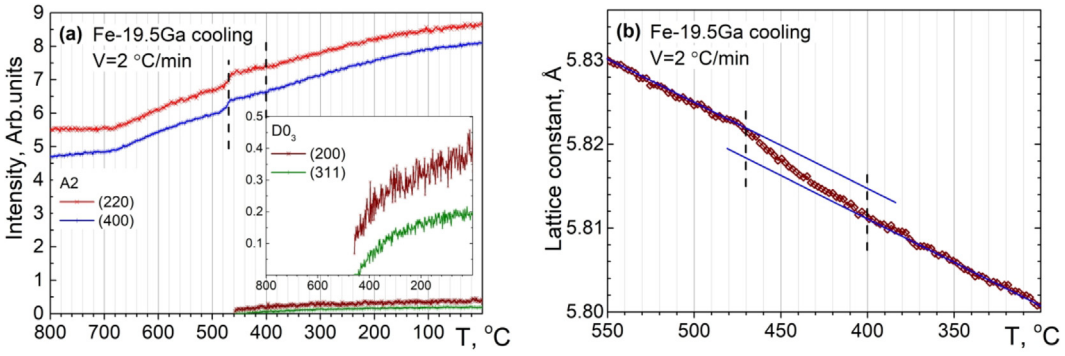

Fig. 1. (a): Intensities of the two fundamental peaks (2 2 0) and (4 0 0) as a function of temperature at cooling with a rate of 2 °C/min for the Fe-19.5 Ga alloy. Intensities of the superstructural peaks (2 0 0) and (3 1 1) with a larger scale in the inset. (b): The lattice constant a(T) of the D03 phase determined from the (2 2 0) diffraction peak position. The vertical dashed lines represent the ordering starting and finishing temperatures.

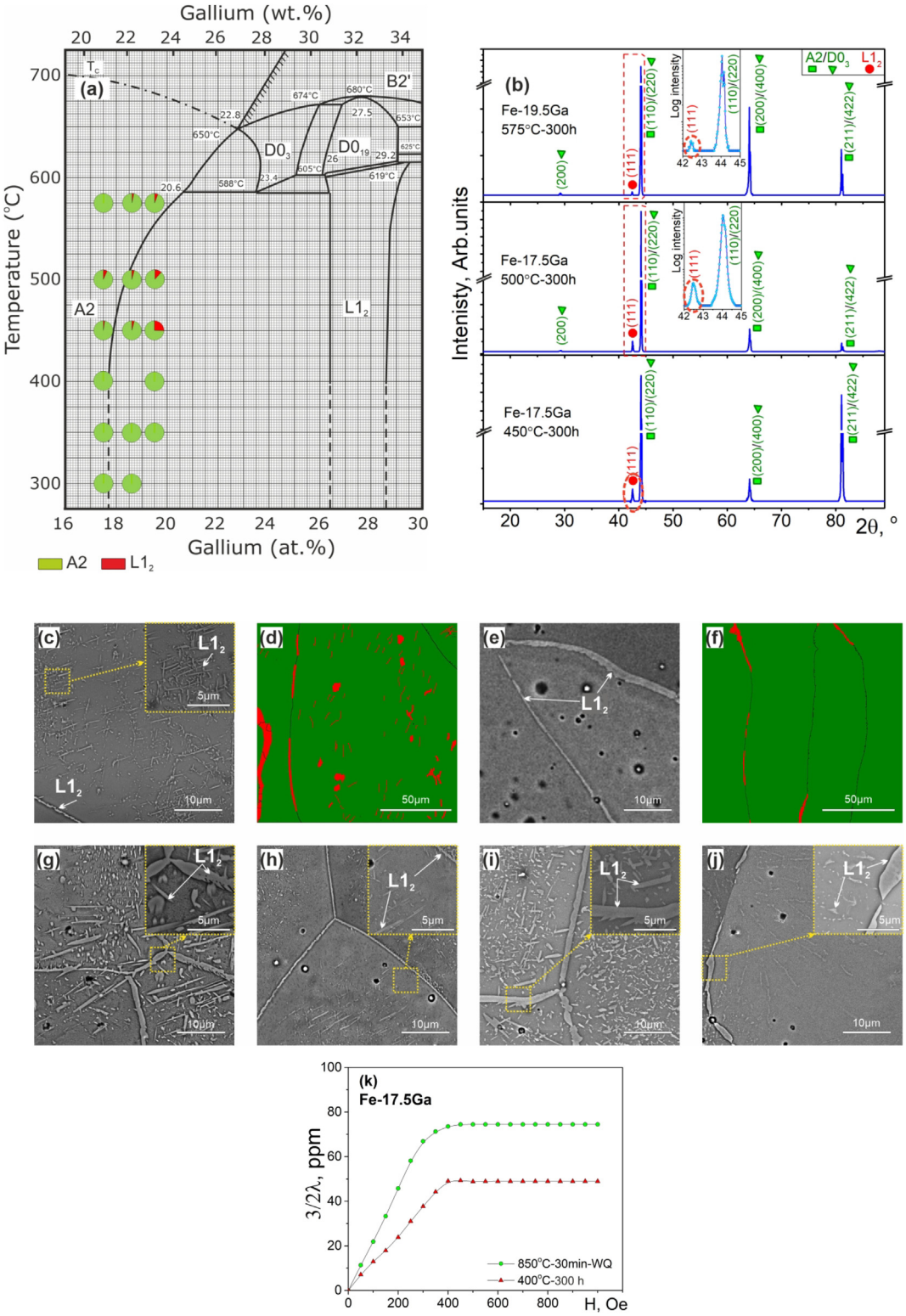

Fig. 2. (a) Fe-Ga equilibrium phase diagram [9] with experimental points illustrating the ratio between the A2($D0_3$) and A1($L1_2$) phases after 300 h annealing. (b) XRD patterns for the 300 h annealed Fe-17.5 Ga at 450, 500 °C and Fe-19.5 Ga at 575 °C samples. (c),(d) SEM-EBSD images for the 300 h annealed samples for Fe-17.5 Ga at 450 °C and (e),(f) for Fe-18.6 Ga at 575 °C. (g) SEM images for the 300 h annealed samples Fe-18.6 Ga at 500 °C, (h) Fe-19.5 Ga at 450, (i) 500, and (j) 575 °C. Green and red colors represent A2($D0_3$) and $L1_2$, respectively. (k) Magnetostriction (3/2λ) results for quenched Fe-17.5 Ga alloy and after 300 h annealing at 400 °C.

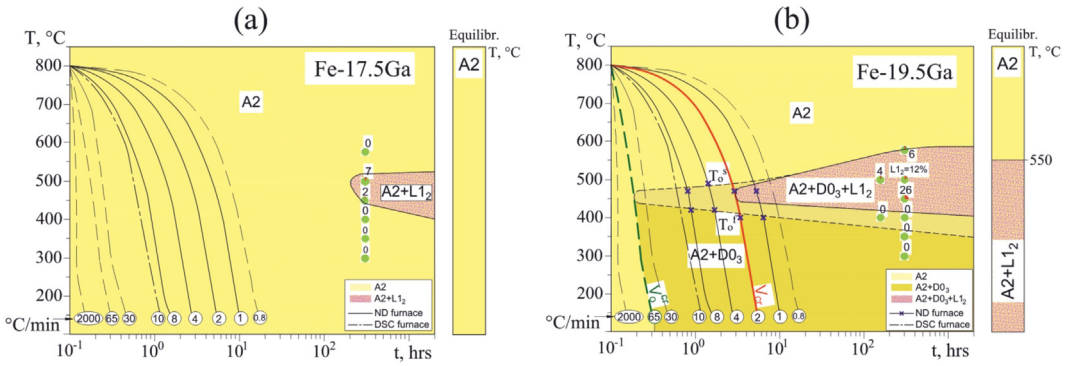

Fig. 3. TTT diagrams for Fe-17.5 Ga (a) and Fe-19.5 Ga (b) alloys. The bar beside the TTT diagrams represents the equilibrium phase temperature ranges [9]. Red, light, and dark yellow areas represent A2 + $D0_3$ + $L1_2$, A2, and A2 + $D0_3$.

magnetostriction was recorded. The following outcomes can be determined:

1. All the investigated as-cast alloys have a single A2 phase in the as-cast state. Cooling from A2 range (850 °C) with cooling rates of 1–8 °C/min leads to ordering A2 → $D0_3$ + A2, according to our *in situ* ND tests. Some traces of the A1 phase also appear after cooling with rates of 1 and 2 °C/min.
2. The studied alloys show the appearance of the $L1_2$ phase fractions after long-term annealing. Even the 17.5%Ga alloy shows precipitates of the $L1_2$ phase after 300 h annealing at 450–500 °C in contrast with the existing phase diagrams. The formation of needle-shaped $L1_2$ precipitations decreases the alloy's magnetostriction. The existing phase diagrams must be corrected in view of these new results. As the next step, the authors plan to apply 1000 h annealing to define the diagram better.
3. The critical cooling rate for starting the first-order transition A2 → $L1_2$ ($\leq$1%) in the Fe-19.5 Ga alloy is about 2 °C/min. For the Fe-17.5 Ga alloy, only long-term annealing helps to define the time–temperature position for the nose's path for the TTT curve.

CRediT authorship contribution statement

A.K. Mohamed: Conceptualization, Validation, Formal analysis, Investigation, Writing - original draft, Visualization. **V.V. Cheverikin:** Investigation. **S.V. Medvedeva:** Data curation. **I.A. Bobrikov:** Investigation. **A.M. Balagurov:** Methodology, Data curation, Writing - review & editing. **I.S. Golovin:** Conceptualization, Validation, Writing - review & editing, Supervision, Project administration.

Declaration of Competing Interest

The authors declare that they have no known competing financial interests or personal relationships that could have appeared to influence the work reported in this paper.

Acknowledgements

The work was supported by the Russian Science Foundation (project No. 19-72-20080). The experiments were carried out using the IBR–2 (JINR) neutron source. A.K.M. gratefully acknowledges the financial support of the Ministry of Education and Science of the Russian Federation in the framework of Increase Competitiveness Program of MISiS. We are grateful to Mr Yavar Mansouri for help with magnetostriction test and Dr. Elena Bazanova for critical reading of this manuscript.

References

[1] A.E. Clark, J.B. Restorff, M. Wun-Fogle, T.A. Lograsso, D.L. Schlagel, IEEE Trans. Magn. 36 (2000) 3238–3240.
[2] J.R. Cullen, A.E. Clark, M. Wun-Fogle, J.B. Restorff, T.A. Lograsso, JMMM. 948 (2001) 226–230.
[3] E. Hristoforou, A. Ktena, S. Gong, Trends IEEE Trans. Magn. 55 (2019) 1–14.
[4] Q. Xing, Y. Du, R.J. McQueeney, T.A. Lograsso, Acta Mater. 56 (2008) 4536–4546.
[5] I.S. Golovin, A.M. Balagurov, A. Emdadi, V.V. Palacheva, I.A. Bobrikov, et al., Intermetallics. 100 (2018) 20–26.
[6] I.S. Golovin, V.V. Palacheva, A.K. Mohamed, A.M. Balagurov, Fizika Metallov i Metallovedenie. 121 (2020) 937–980.
[7] I.S. Golovin, A.M. Balagurov, I.A. Bobrikov, S.V. Sumnikov, A.K. Mohamed, Intermetallics. 114 (2019) 106610.
[8] I.S. Golovin, A.K. Mohamed, I.A. Bobrikov, A.M. Balagurov, Materials Letters 263 (2020) 127257.
[9] O. Kubaschewski Iron-Binary Phase Diagrams 1982 Springer Berlin Heidelberg, Berlin, Heidelberg
[10] A.M. Balagurov, Neutron News 16 (2005) 8–12.
[11] S.U. Jen, Y.Y. Lo, L.W. Pai, J. Phys. D: Appl. Phys. 49 (2016) 145004.
[12] A.K. Mohamed, V.V. Palacheva, V.V. Cheverikin, E.N. Zanaeva, W.C. Cheng, V. Kulitckii, S. Divinski, G. Wilde, I.S. Golovin, J. Alloys Compd. 846 (2020) 156486.
[13] W. Köster, T. Gödecke, Z. Metallk. 68 (1977) 661–666.
[14] J. Bras, J.J. Couderc, M. Fagot, J. Ferre, Acta Metallurgica. 25 (1977) 1077–1084.
[15] H. Okamoto, Binary Alloy Phase Diagrams, 2nded., ASM International: Materials Park, USA, 1993.
[16] M. Sun, X. Wang, L. Wang, H. Wang, W. Jiang, et al., J. Alloys Compd. 750 (2018) 669–676.
[17] A.M. Balagurov, I.A. Bobrikov, I.S. Golovin, JETP Letters 110 (9) (2019) 585–591.
[18] A.M. Balagurov, N. Samoylova, I.A. Bobrikov, S.V. Sumnikov, I.S. Golovin, Acta Cryst. B. 75 (2019) 1024–1033.
[19] O.I. Noskovich, E.I. Rabkin, V.N. Semenov, B.B. Straumal, L.S. Shvindlerman, Acta metall. mater. 39 (1991) 3091–3098.
[20] I.S. Golovin, A.M. Balagurov, W.C. Cheng, J. Cifre, D.A. Burdin, Intermetallics 105 (2019) 6–12.